

UC Santa Barbara

UC Santa Barbara Previously Published Works

Title

Phosphorus stimulated unidirectional growth of TiO₂ nanostructures

Permalink

<https://escholarship.org/uc/item/74p088n9>

Journal

Journal of Materials Chemistry A, 1(19)

ISSN

2050-7488

Authors

White, Lauren M
Kim, Myung Hwa
Zhang, Jinping
[et al.](#)

Publication Date

2013

DOI

10.1039/c3ta01403g

Copyright Information

This work is made available under the terms of a Creative Commons Attribution-NonCommercial-NoDerivatives License, available at <https://creativecommons.org/licenses/by-nc-nd/4.0/>

Peer reviewed

Phosphorus stimulated unidirectional growth of TiO₂ nanostructures

Lauren M. White¹, Myung Hwa Kim², Jinping Zhang³, Stephan Kraemer,⁴ Cafer T. Yavuz⁵, ,
Martin Moskovits¹, Alec M. Wodtke^{1,6,7}, and Galen D. Stucky*^{1,4}

1. *Department of Chemistry & Biochemistry, University of California at Santa Barbara*

2. *Department of Chemistry & Nano Science, Ewha Womans University, Seoul 120-750, Korea*

3. *Suzhou Institute of Nano-Tech & Nano-Bionics, Chinese Academy of Sciences, Suzhou
215125, China*

4. *Materials Department, University of California at Santa Barbara*

5. *Graduate School of EEWS, KAIST, Daejeon, 305-701, Republic of Korea*

6. *Institute of Physical Chemistry, Georg-August University of Göttingen, Germany*

7. *Department of Dynamics at Surfaces, Max-Planck Institute for Biophysical Chemistry,
Göttingen, Germany*

* To whom all correspondence should be addressed: stucky@chem.ucsb.edu

Abstract

Previously reported TiO₂ nanowire fabrication from Ni catalysts shows a surprising amount of phosphorous (P) contamination incorporated into the seed particle. We proposed this unintentional P-doping of Ni particles aids the mechanism for nanowire growth and occurs by an alternative pathway from the Vapor-Liquid-Solid (VLS) mechanism. To confirm this new mechanism, mixed phase NiP/Ni₂P (Ni_xP_y) and Ni₂P nanoparticles were fabricated and the central role of phosphorous in TiO₂ nanowire synthesis confirmed. This newly developed P-assisted fabrication method yielded crystalline rutile TiO₂ nanowires. In this mechanism solid, quasi-spherical catalyst particles attached to the ends of nanowires and surrounded by a Ni/P liquid shell are responsible for the nanowire growth. The growing end of the nanowire appears to form a “tangent-plane” to the solid catalyst core with the liquid shell wetting and occupying the interstice between the catalyst and the nanowire. In Ni_xP_y assisted growth, nanowire diameters occurred as small as 12.3nm, some of the thinnest yet reported TiO₂ nanowires resulting from atmospheric-pressure chemical vapor deposition (APCVD) growth.

Introduction

Recent investigations of titanium dioxide nanowires (NWs) highlight these nanostructures as attractive candidates for gas sensors, charge transport materials in photovoltaic devices, and photocatalysts.¹⁻⁴ Specifically, rutile phase TiO₂ nanowires have been studied for excellent charge transport capabilities and high surface area and tested as anode materials to improve lithium ion batteries.⁵ Titanium dioxide (TiO₂) has achieved large scale real-world applications due to its low cost, low toxicity and because it is environmentally safe. Currently, typical nanowire syntheses methods include atmospheric-pressure chemical vapor deposition (APCVD).^{6,7} However, optimization of growth conditions, and hence bulk production, is difficult since their growth mechanism is still uncertain. Wagner and Ellis (1964) first recognized the Vapor-Liquid-Solid (VLS) mechanism for nanowire fabrication as being the primary pathway for growth. VLS growth utilizes catalytic metal nanoparticles (NPs) that form low-melting point eutectic alloys with one of the reactants.⁸ The liquid catalyst nanodroplet ultimately becomes the nucleus on which preferential and unidirectional crystal growth occurs. In addition, subsequent research provided evidence of alternative mechanisms such as Vapor-Solid-Solid (VSS)^{4,6} and Solid-Liquid-Solid (SLS)⁹ where nanowire growth occurs well below the expected melting point of the catalyst nanoparticles. Furthermore, recent reports by Kim et al. describe another variation of the growth mechanism which they describe as "tangent plane growth."⁸

Previously, we reported that an unexpected amount of phosphorus impurity was involved in APCVD growth of TiO₂ nanowires.⁸ In those experiments, a 2nm film of Ni was annealed onto a Ti/Si substrate where the Ni film was the catalyst (seed particle) for nanowire growth. Despite the fact that phosphorus was not intentionally added in those experiments, high resolution transmission electron microscopy (HRTEM) revealed post-growth catalyst particles composed of a solid Ni core with an outer shell of Ni₃P. Since highly crystalline rutile TiO₂ nanowires were grown from these phosphorus-contaminated Ni catalysts, we hypothesized that phosphorus, and possibly other dopants, could be enhancing the growth mechanism.

In this work, we report the results of using synthesized Ni/P alloys for fabricating TiO₂ nanowires by APCVD. Specifically, the goal is to understand the role of phosphorus in the TiO₂ nanowire growth mechanism by using mixed phase NiP/Ni₂P and Ni₂P nanoparticles under growth conditions similar to those used in previous experiments. Furthermore, we compare the

resulting nanowire growth by the intentional addition of phosphorus to those obtained previously in order to obtain a better understanding of the growth mechanism. In our previous work, we showed unintended P-impurities exhibited a remarkable influence on TiO₂ nanowire growth. In the work presented here, we have carried out the first attempts to introduce P-doping in a controlled way to intentionally introduce a new avenue of control over TiO₂ nanowire growth. By doing so we are able to demonstrate comparatively smaller nanowire diameters and control over TiO₂ phase (consistently rutile phase). We show P-doping has a positive influence on the control and fabrication of TiO₂ nanowires and suggest that this method may be optimized and tuned for a variety photovoltaic and sensing applications.

Experimental Section

Synthesis of NiP/Ni₂P solid crystalline nanoparticles. Initially, we synthesized solid crystalline NiP/Ni₂P nanoparticles (referred to as Ni_xP_y for brevity) following a similar procedure to that reported by Chiang and Chiang.¹⁰ This is a one pot synthesis of Ni_xP_y nanoparticles that uses nickel acetate (tetrahydrate, 1mmol)[Sigma Aldrich], trioctylphosphine oxide (TOPO) (10mmol) [Sigma Aldrich], oleylamine (20mmol)[Sigma Aldrich 70%], trioctylphosphine (TOP) (2mmol) [Sigma Aldrich 90%] and a growth temperature of 250°C under inert atmosphere for 1 hr. The resulting nanoparticles are precipitated out of solution by several sequential additions of acetone and subsequent centrifuging. NPs were vacuum dried overnight and resuspended in hexane.

Synthesis of Ni₂P solid crystalline nanoparticles. For Ni₂P synthesis, we followed the procedure outlined by Wang et al.¹¹ where 0.200g (0.778mmol) nickel acetylacetonate [Ni(acac)₂, 98%, Sigma-Aldrich] and 2.0ml (6.1mmol) oleic acid (90%, Sigma-Aldrich) was added to 5.0mL (15.7mmol) of 1-octadecene (ODE, 90%, Sigma-Aldrich) in a three-necked, round-bottomed flask. The solution was heated to 80°C while stirring until the solution became transparent. After degassing at 80°C for 2hr and backfilling with argon, 5.0mL of TOP (97%, Stem Chemical) were added by syringe. The temperature was rapidly increased to 300°C for another 30 min to completely convert particles to crystalline-solid Ni₂P nanoparticles.

The solution was then allowed to cool to room temperature whereupon ~30mL acetone were added to the flask in order to precipitate the nanoparticles, followed by centrifugation to separate them from the solvent. The acetone was decanted off and one part hexane and three parts MeOH

were added to the centrifuge tube directly followed by centrifugation to flocculate and further separate the NPs from the solvent. Nanoparticles were repeatedly (3-5 times) reflocculated and separated by MeOH/hexane washes and centrifugation. The NPs were dried overnight under vacuum and stored in hexane.

TiO₂ nanowire substrate preparation. For TiO₂ nanowire growth, a 50nm Ti layer was deposited by electron-beam evaporation onto a Si/SiO₂ wafer [Si <100> with a 200nm thick thermally grown SiO₂ layer, SQI]. For all solutions of Ni_xP_y and Ni₂P nanoparticles dispersed in hexane, approximately 3 drops of colloidal nanoparticle solution were spin coated onto the Si/SiO₂/Ti substrate at 3000 rpm for 40 sec using a *WS-400-6NPP-LITE* spin coater. The number of drops of solution was held constant while the NP concentration was varied to observe effects of nanoparticle surface concentrations on nanowire growth.

CVD nanowire growth. NW growth was carried out in a horizontal quartz tube furnace, 2.5cm in diameter and 122cm long. Approximately 0.2g of Ti(II)O mesh (99.95%, Sigma-Aldrich) were placed ~5mm upstream from prepared substrates in the center of a quartz boat. The quartz boat was situated at the center of the quartz tube furnace and heated to 950°C in air for ~10min and maintained at 950°C for another 10 min. APCVD growth was carried out for 2 hr under flowing high-purity Ar (99.998%) at 300 sccm. For analysis by transmission electron microscopy (TEM), substrates containing nanowires were sonicated for 60 sec in 1ml EtOH and added dropwise to a 200 mesh carbon coated copper TEM grid.

Nanoparticle and Nanowire Analysis. The resulting nanowires were observed directly on the Si/Ti substrate by scanning electron microscopy (SEM) using a FEI XL40 Sirion FEG microscope with attached Oxford Inca X-Ray system for energy dispersive spectroscopy (EDS). The parameters used for obtaining high resolution SEM images were: 5kV electron energy, working distance of 5mm and 98 pA electron current. EDS spectra were obtained using an electron energy of 20kV, a point dwell time of 60 sec and a 62 nA electron current. Semi-quantitative atomic weight percent values were calculated using INCA microanalysis software. TEM images and selected area electron diffraction (SAED) patterns were obtained using a FEI Tecnai G2 Sphera Microscope. Scanning TEM imaging (STEM), Bright Field (BF) TEM imaging, EDS, and EDS line scans were obtained using FEI Titan 80-300 FEG High Resolution TEM/STEM and analytical microscope.

Results

Synthesis and Analysis of Ni_xP_y nanoparticles. NiP/Ni₂P (Ni_xP_y) nanoparticles were synthesized according to the procedure outlined in the experimental section. Three varying concentrations (~1.00 wt%, 2.00 wt% and 7.50 wt %) of Ni_xP_y in hexane solution were spin coated onto three identically prepared Si/SiO₂/Ti wafers. APCVD nanowire growth was attempted on all three samples with similar conditions as described in the experimental section for all three substrates. In addition, it should be noted that CVD growth conditions for new phosphorus-assisted growth are similar to those described in earlier work.⁷

Atomic force microscopy (AFM) (supplemental information S1) and TEM imaging confirmed a solid structure for the resulting Ni_xP_y nanoparticles and average diameters ranging from 10-12nm (Fig. 2). TEM and EDS analysis confirmed the nanoparticles synthesized were composed of Ni and P (supporting material S2). SAED patterns collected over the nanoparticles confirmed a crystalline Ni₂P¹² composition mixed with NiP¹³ (supplemental information S3).

Ni_xP_y Assisted Growth. The three concentrations of Ni_xP_y in hexane were spin coated onto three Si/SiO₂/Ti substrates prepared under identical conditions. Nanowire fabrication was attempted on all three samples using the previously described APCVD method where all samples were heated to 950°C. Figure 3 shows HRSEM images of the resulting nanowire growth. Analysis of these images confirms that the lowest concentration of Ni_xP_y on the surface of the substrate produces the least amount of nanowire growth and as the concentration of Ni_xP_y is increased the number of nanowires grown on the surface increases. Because the same amount of solution was used to spin coat all three substrates for all three solutions, the lowest concentration of Ni_xP_y in solution likely results in a lower number of seed particles on the substrate surface. Therefore, fewer seeds are available for growth and relatively fewer nanowires are observed for the lowest Ni_xP_y solution concentration (1.00 wt%). More importantly, uniform high quality TiO₂ nanowire growth is facilitated, and not inhibited by, the addition of phosphorus to the catalyst particle. Typically, nanowire growth by chemical vapor deposition is thought to occur by the VLS mechanism where the diameter of the nanowires is closely controlled by the diameter of the starting catalytic particle.¹⁴ Since all three samples were spin coated with Ni_xP_y nanoparticles from the same batch but with differing concentrations, one might expect to see similar diameters of nanowire growth for all three substrates. However, as shown in figure 3, the average diameter

of the TiO₂ nanowires increases from 12-20nm (Fig. 1 & 3b) for 2.00 wt % Ni_xP_y to 30-80nm for 7.50 wt % Ni_xP_y. Since the increasing wt % of Ni_xP_y translates into nanoparticles resting closer together on the substrate surface, the increasing nanowire diameter may result from increased NP aggregation with increasing nanoparticle surface concentration, i.e. NPs may be more likely to aggregate to form particles with larger diameters (greater than 10-12nm) during the initial heating step before nanowire growth occurs. Thus, subsequent nanowire growth from large catalyst particles leads to larger nanowire diameters. Energy dispersive X-Ray spectroscopy (EDS) on resulting nanowires revealed the presence of Ni and P in the catalyst particle and Ti and O in the nanowires. EDS spectra showed a semi-quantitative Ni:P atomic % ratio of nearly 3:1 (Fig. 4) - a similar ratio to the crystalline Ni₃P catalytic particles produced by CVD growth on the ends of TiO₂ nanowires that prompted the present investigation.⁸ Measured g vectors from TEM diffraction patterns obtained for nanowires matched those of rutile TiO₂ (Fig. 5). This result is consistent with previous phosphorus contaminated experiments where the TiO₂ nanowires produced were also found to be rutile phase.⁸

It should be noted that while Ni_xP_y batches synthesized by the same procedure (i.e. similar to that of Chiang and Chiang¹⁰) usually produced similar nanowire growth on Si/SiO₂/Ti substrates, other batches yielded amorphous head particles with higher occurrence of kinks and bends in the resulting nanowires. To better understand this, we performed TEM imaging on nanoparticles that led to kinked nanowire growth. Images revealed that the nanoparticles produced formed a mixture of both hollow and solid crystalline phases (supplementary info S4). Since our previous results suggested that a core-shell structure facilitates the nanowire growth through the transport of materials to the surface of the substrate,⁸ we conclude here that the hollow nanoparticles were inhibiting the nanowire growth and causing the kinked structures observed. We determined that the procedure outlined in the experimental methods section, as well as the nanoparticle synthesis outlined by Chiang and Chiang¹⁰, does not consistently produce solid crystalline NPs but occasionally yields a mixture of both solid crystalline as well as hollow crystalline NPs. This result is supported by subsequent research by Wang et al.¹¹ describing similar mixtures of hollow and solid nanoparticles when following the Chiang and Chiang¹⁰ procedure. Wang et al.¹¹ addresses the problem by conducting a series of experiments that lead to more controlled methods of producing exclusively hollow or solid nanoparticles. They report the fabrication of crystalline solid Ni₁₂P₅/Ni₂P nanoparticles exclusively (with no hollow NPs) by adjusting the

reactant P:Ni ratios as well as the temperature ramp sequence and solvent. Therefore, following the procedure outlined by Wang et al.¹¹, solid crystalline Ni₁₂P₅/Ni₂P NPs were fabricated for use as catalysts to further investigate phosphorus-assisted TiO₂ nanowire growth. Moreover, we sought to observe the effect of changing the concentration of phosphorus in the nanoparticle (NiP/NiP₂ versus Ni₁₂P₅/Ni₂P), on nanowire growth. This was undertaken using identical substrates and growth conditions (950°C) as in previous experiments with Ni_xP_y.

Analysis of Ni₁₂P₅/Ni₂P. Upon synthesis of Ni₂P solid crystalline nanoparticles, four dilutions of Ni₂P in hexane were prepared for spin-coating onto Si/SiO₂/Ti substrates, 14.26 wt%, 7.13 wt %, 3.56 wt% and 1.78 wt%. A dilute solution of Ni₂P dispersed in hexane was also added dropwise onto a 200 mesh carbon coated copper grid for later TEM analysis.

EDS and SAED were used to confirm the crystal structure of the synthesized seed particles following the work of Wang et al.¹¹ EDS spectra revealed that nanoparticles are composed of Ni and P (supplementary info S5). Cu and carbon peaks observed on EDS spectra can be attributed to background from the TEM grid. Measured g vectors from synthesized nanoparticle SAED patterns appear to fall mainly on values for Ni₂P, suggesting the Ni₁₂P₅/Ni₂P mixture is primarily Ni₂P (supplementary info S6). This result is further supported by the Ni-P binary phase diagram which indicates a relatively narrow compositional range for pure Ni₁₂P₅ directly adjacent to the formation of Ni₂P (Fig. 9). Therefore we refer to the Ni₁₂P₅/Ni₂P mixture as Ni₂P for clarity.

Ni₂P Assisted Growth. Nanowire fabrication was attempted for all four dilutions of NPs (as described above) under identical CVD conditions as described in the Experimental Methods section. Similar to Ni_xP_y assisted growth, the greatest occurrence of nanowire growth resulted from the highest concentration of particles (14.26 wt%) and no nanowires were observed for the lowest (1.78 wt%) concentration of Ni₂P. However, nanowire diameters grown from Ni₂P seeds exhibited a wider range compared to Ni_xP_y growth, with diameters from 26-161±5 on the 14.26 wt% substrate. Nevertheless, average diameters are similar to those observed on the ~7.50 wt % Ni_xP_y substrate, ranging from ~50-80±2nm (Fig. 6). The diameters of nanowires and their corresponding attached catalyst particle were obtained from SEM analysis. We note in one example (supplemental information S7) that two different catalyst particle diameters (197nm and 470nm) yielded closely similar nanowire diameters (85.4nm and 88.9nm respectively).

High resolution STEM imaging and EDS analysis revealed non-homogeneous compositions in some nanowires produced from Ni₂P batch solutions. Shown in figures 6 & 7, most nanowires were confirmed to be the TiO₂ rutile phase. Semi-quantitative data from EDS line scans suggest a TiO_x NW composition and a Ni-P spherical catalyst (Fig. 8a). Moving from left to right across the ~20nm line shown in Fig. 8b, EDS spectra reveal a relatively high abundance of Ti and O (68.48 % and 31.52 % respectively) while the signal from Ni and P are nearly zero. Near the center of the particle and away from the nanowire, the composition shifts along the line to mostly Ni-rich with Ni, P, Ti and O signals amounting to 83.66 %, 2.28 %, 0.98 % and 3.45% respectively. Si was also observed (9.62% abundance near the center of the particle) in the amorphous shell of this catalyst particle. Although abundant in the shell observed in figure 8, Si was observed only in some particles (roughly half of those analyzed by EDS) while in others it was completely absent. The reduced signals from Ti and O at the end of the line nearest to the center of the catalyst particle are comparable to those observed in Ref. 7 and suggest that an oxygen-rich material forms a shell around the nanoparticle. The spectrum collected over the interface region between nanowire and nanoparticle (from 11-20nm) shows a steep increase in oxygen content at the interface where the ratio of oxygen to titanium approaches to nearly 2:1. Complementary HRTEM imaging over this oxygen-rich region indicates that the material is amorphous and extends around the entire exterior surface of the catalyst. The Ti signal also shows a similar steep increase near the same region on the line (4-20nm). This amorphous Ti-O-P containing shell is consistent with previous line scans over phosphorus-contaminated particles.⁸ This core-shell structure is also consistent with recent studies on Ni-P nanoparticles which form core-shell structures depending on the relative kinetics of each migrating species (Ni and P).¹³

Measured g vectors from SAED patterns obtained during TEM analysis of post-growth nanowires suggest that the seed particles are solid Ni (supplementary information S8). Although no phosphorus was observed by SAED, EDS line scan spectra obtained on the same Ni seeds show an increasing amount of phosphorus in the outermost layer of the nanoparticle as compared with the interior (supplementary information S9). Thus, EDS analysis in combination with SAED results suggests that the post-nanowire growth catalysts are composed of a solid Ni core with an outer phosphorus/nickel shell, similar to that reported in Ref. 7.

In some Ni₂P derived nanowires, EDS indicated catalyst particles were solid crystalline Ni with no observable phosphorus content and an outer shell of amorphous Ni-O. This result is similar to the amorphous Ni-Ti-O shell seen in Ref. 7. SEM and STEM imaging show spheroidal structures protruding from the surface of other Ni₂P derived nanowires. EDS spectra collected on these structures indicate that these spheroids are the result of phosphorus erupting outward from the particle and solidifying on the outer surface of the resulting solid Ni catalyst (Fig. 7). In some rare cases, we also observe nanoparticles at the ends of NWs with a hexagonal structure and EDS-calculated Ni:P ratios of 2:1. This ratio and hexagonal shape indicates a typical hcp structure for Ni₂P suggesting that some Ni₂P seed particles may remain unchanged during the nanowire growth process.

The mechanism indicated by nanowire and seed particle structures appears to be the same in both Ni_xP_y and Ni₂P assisted growth with the resulting seed particles remaining nearly spherical for unidirectional nanowire growth. This ball-and-stick structure differs from the typical VLS structure where catalyst particles are quasi-hemispherical with a greater surface area exposed to the direction of nanowire growth. A fully spherical structure is exhibited by our P-assisted nanowire growth and is strikingly similar to our previously proposed “tangent-plane” mechanism in P-contaminated experiments.⁸ Furthermore, the amorphous shell of material observed at the interface between the nanowire and catalyst, as seen by TEM and STEM imaging (Fig. 7 and 8), suggests a solid nickel core surrounded by a shell of Ni-P. The solid Ni core structure precludes the collapse of the catalyst particle into a quasi-hemispherical shape typical of VLS, while the liquid shell provides the active (and efficient) reaction medium. As expected based on the data given in the Ni-P phase diagram, the Ni/P mixture has a lower melting point than that of pure Ni (Fig. 9).

Discussion

In light of previously discovered phosphorus impurities in our seed particles,⁸ we intentionally incorporated phosphorus into the catalyst particle in order to experimental test our previously suggested hypothesis that phosphorus may be important in facilitating TiO₂ nanowire growth. New experiments include nickel-phosphide catalysts, mixed phase NiP/Ni₂P (Ni_xP_y) and Ni₂P nanoparticles. Nanowire growth appeared similar in both Ni_xP_y and Ni₂P growth except in cases

where hollow Ni_xP_y nanoparticles occurred. In both cases, we observe the formation of rutile phase TiO_2 nanowires and quasi-spherical seed particles attached to the ends of nanowires.

Seeding TiO_2 with Ni_xP_y nanoparticles resulted in highly crystalline rutile phase nanowires. By increasing the number of particles dispersed onto the substrate surface we saw a general trend of increasing nanowire growth both with respect to diameter and length. In the case where ~ 2.00 wt % Ni_xP_y in hexane was spin-coated onto the substrate, TiO_2 nanowires as narrow as $\sim 12\text{nm}$ across were observed. To the best of our knowledge, this is the thinnest diameter yet reported for TiO_2 nanowires grown by APCVD. Where NP batches were later found to contain a mixture of hollow and solid particles, poor nanowire growth resulted with amorphously shaped seed particles and non-unidirectional nanowire growth.

In order to control the starting crystallinity of catalyst particles and observe any changes in nanowire growth with changes in the Ni-P phase (Ni_xP_y versus Ni_2P), we attempted similar CVD nanowire growth using Ni_2P nanoparticles as catalysts. In Ni_2P assisted growth, we again observed higher density nanowire growth in the case where the highest wt % of Ni-P NPs in hexane solution was used. As seen in Ni_xP_y and Ni-film experiments, the resulting TiO_2 nanowire growth appears unidirectional with quasi-spherical seed particles surrounded by an amorphous outer shell. Overall, the range of nanowire diameters appears much larger in Ni_2P compared to Ni_xP_y assisted growth. However, Ni_2P assisted growth yielded more consistently uniform nanowire growth with fewer cases of amorphous shapes or kinks in wires as observed in Ni_xP_y growth experiments.

In addition to Ni-P nanoparticle experiments, we also performed experiments without the intentional addition of phosphorus. Using different quartz tubes and high purity quartz boats, we performed effectively phosphorus-free TiO_2 nanowire growth under the same conditions (950°C). In this experiment we used identical substrates (Si/ SiO_2 and 50nm Ti layer) and titanium source (titanium mesh) as for those described for the Ni-P nanoparticle experiments. The Ni-P nanoparticles were replaced with a 2nm Ni layer (as used in previous non-phosphorus doped experiments⁸). As described previously,⁸ TiO_2 nanowire growth was suppressed and no well-formed head particles or nanowires were observed (data not shown). This observation, in combination with data from the phosphorus-doped experiments described here, suggests phosphorus facilitates highly crystalline TiO_2 nanowire growth.

At present, Vapor-Liquid (VLS) growth is the most common method for producing large quantities of high quality nano-materials. However, many attempts have recently been made to challenge the growth mechanism originally proposed by Wagner and Ellis in 1964.^{15, 16} In our previous work, we presented evidence for tangent-plane growth where the seed catalyst particle remains spherically intact and an amorphous shell of Ti-Ni-O material surrounds the exterior of the nanoparticle as well as the interface region between nanowire and seed.⁸ We also clearly presented a case for trace element, P, appearing on the surface of a designed Ni catalyst particle. We showed that high quality TiO₂ nanowires could grow on solid (phosphorus-doped) Ni at 950°C, a temperature far below the typical melting point of 1455°C for bulk Ni (or of the Ni nanoparticle).

In the experiments we report here, we show consistently similar rutile TiO₂ nanowire growth at the same temperature (950°C) using phosphorus-doped nickel nanoparticles. EDS line scans through the interface area between the nanoparticle and nanowire indicate an amorphous, oxygen-rich material which forms a shell on the outer surface of a quasi-spherical NP. HRTEM images and SAED patterns collected on the catalyst particle after nanowire growth reveal a solid Ni phase with an amorphous shell on the outer surface. The binary phase diagram (Fig. 9) indicates a eutectic temperature of the Ni-P that is 891°C, well below our working temperature of 950°C. The amorphous shell and quasi-spherical shape observed in our Ni-P seeds suggest that the mechanism for growth includes the formation of a liquid Ni-P shell (in agreement with the Ni-P phase diagram) which surrounds a solid Ni core. These results are consistent with the tangent-plane mechanism proposed previously in experiments where unintentional addition of phosphorus was hypothesized to aid in TiO₂ nanowire synthesis.⁸ In this mechanism, the liquid shell and solid core together act as the catalyst for adsorption, diffusion, and reaction of Ti and O, resulting in TiO₂ nucleation and crystallization from the liquid phase near the surface of the solid nickel nanoparticle.⁸ Formation of a typical VLS-growth quasi-hemispherical shape is inhibited by the solid Ni core while the liquid shell provides the active reaction medium. Furthermore, unlike typical VLS growth where the diameter of the nanowire is limited by the diameter of the starting catalyst,¹⁷ we observed nanowires of similar size grown from different diameters of Ni₂P nanoparticles.

Conclusion

This research confirms in more detail the facilitation of TiO₂ nanowire growth by means of phosphorus catalysis. Furthermore, through repeated experimentation, we show a novel phosphorus doping method for fabricating rutile TiO₂ nanowires. By incorporating phosphorus into the catalytic nanoparticle, APCVD nanowire growth is accomplished by an alternative process to the vapor-liquid-solid mechanism. The observed quasi-spherical nanoparticle shape appears similar to our previously proposed “tangent-plane” mechanism.⁸ When phosphorus is removed, TiO₂ nanowire growth is suppressed and no quasi-spherical seed particles are observed. This novel method of P-assisted TiO₂ nanowire growth consistently results in rutile phase TiO₂ nanowires. As noted earlier, rutile TiO₂ is regarded as promising for lithium insertion/extraction materials due to its low production cost and high capacity for lithium intercalation.^{5, 18} In addition, we report significantly smaller nanowire diameters (down to 12nm) produced from the P-assisted method compared to previous non P-assisted experiments. Such small diameters would be useful particularly in gas sensing devices. For example, Moskovits et al. (2010) recently developed an “electronic nose” device comprised of decorated metal-oxide nanowires providing improved sensitivity toward carbon monoxide, hydrogen and ethylene over bulk materials due to the higher surface area of the catalyst. Compared to previously reported nanowire synthesis, the P-assisted method similarly produces rutile phase TiO₂ nanowires but smaller diameters depending on Ni-P seed particle used. Except where hollow nanoparticles were present, TiO₂ nanowire fabrication from Ni-P seeds was consistent for both amounts of P tested. Therefore, these results suggest trace elements which may be present in VLS nanowire growth should not be ignored and can have a positive influence on the fabrication method. By taking impurities into account, this work represents a novel example of nanoparticle assisted nanowire growth which is inspired by P impurities. We postulate that a similar P-assisted method could be used for other metal oxide nanowire fabrication in future research.

Acknowledgements

This work was supported by the ConvEne IGERT Program (NSF-DGE 0801627), the PIRE-ECCI Program (NSF-OISE 0530268), NSF-DMR 0805148, and the California Space Grant. Special Thanks to the Suzhou Institute for Nanotechnology and Nanobionics. We also thank Dr

Guang Wu, Department of Chemistry & Biochemistry, UCSB, for discussions regarding XRD analysis of our samples.

References

1. M. Gratzel, *Nature*, 2001, **414**, 338-344.
2. K. R. Thampi, J. Kiwi and M. Gratzel, *Nature*, 1987, **327**, 506-508.
3. A. Kolmakov and M. Moskovits, *Ann. Rev. Mater. Res.*, 2004, **34**, 151-180.
4. J. M. Baik, M. H. Kim, C. Larson, X. H. Chen, S. J. Guo, A. M. Wodtke and M. Moskovits, *Appl. Phys. Lett.*, 2008, **92**, 242111.
5. Z. Wei, H. Mao, T. Huang and A. S. Yu, *J. Power Sources*, 2013, **223**, 50-55.
6. V. Schmidt and U. Gosele, *Science*, 2007, **316**, 698-699.
7. R. S. Wagner and W. C. Ellis, *Appl. Phys. Lett.*, 1964, **4**, 89-&.
8. M. H. Kim, J. M. Baik, J. P. Zhang, C. Larson, Y. L. Li, G. D. Stucky, M. Moskovits and A. M. Wodtke, *J. Phys. Chem. C*, 2010, **114**, 10697-10702.
9. H. F. Yan, Y. J. Xing, Q. L. Hang, D. P. Yu, Y. P. Wang, J. Xu, Z. H. Xi and S. Q. Feng, *Chem. Phys. Lett.*, 2000, **323**, 224-228.
10. R. K. Chiang and R. T. Chiang, *Inorg. Chem.*, 2007, **46**, 369-371.
11. J. W. Wang, A. C. Johnston-Peck and J. B. Tracy, *Chem. Mater.*, 2009, **21**, 4462-4467.
12. A. W. Hull, *Phys. Rev.*, 1921, **17**, 571-588.
13. S. Carenco, X. F. Le Goff, J. Shi, L. Roiban, O. Ersen, C. Boissiere, C. Sanchez and N. Mezaillies, *Chem. Mater.*, 2011, **23**, 2270-2277.
14. H. Okamoto, *J. Phase Equil.*, 2000, **21**, 210-210.
15. S. Kodambaka, J. Tersoff, M. C. Reuter and F. M. Ross, *Science*, 2007, **316**, 729-732.
16. B. A. Wacaser, K. A. Dick, J. Johansson, M. T. Borgstrom, K. Deppert and L. Samuelson, *Adv. Mater.*, 2009, **21**, 153-165.
17. M. H. Huang, Y. Y. Wu, H. Feick, N. Tran, E. Weber and P. D. Yang, *Adv. Mater.*, 2001, **13**, 113-116.
18. B. Han, S. J. Kim, B. M. Hwang, S. B. Kim and K. W. Park, *J. Power Sources*, 2013, **222**, 225-229.

Figure Captions

Figure 1: HRSEM imaging of TiO₂ nanowire grown from Ni_xP_y catalyst confirms 12.3±0.4nm diameter sizes. The scale bar represents 100nm.

Figure 2: BF TEM imaging of Ni_xP_y nanoparticles confirming average 10-12nm diameter sizes (<20nm). The scale bar represents 20nm.

Figure 3: HRSEM imaging shows (a) little to no TiO₂ nanowire growth with ~1.00 wt % Ni_xP_y in hexane solution (b) NWs grown from ~2.00 wt % Ni_xP_y in hexane solution occur 12-30nm in diameter and 2-3µm in length and (c) NWs grown from ~7.50 wt% Ni_xP_y in hexane solution ranging from 30-80nm in diameter and 6-10 µm in length. All Ni_xP_y solutions were dispersed onto a Si/SiO₂/Ti substrate.

Figure 4: EDS analysis of TiO₂ nanowires derived from Ni_xP_y seed particles shows a nearly 3:1 ratio of Ni:P suggesting the particle may contain Ni₃P.

Figure 5: STEM image of fabricated nanowires from Ni_xP_y catalyst particles. The inset shows SAED pattern confirming nanowires are a highly crystalline rutile phase TiO₂ that preferentially grow in the (100) direction.

Figure 6: (a) HRSEM image reveals that a greater quantity of nanowire growth occurs with higher number of Ni₂P particles dispersed onto the surface is increased. (b) HRSEM image showing nanowire diameters are relatively large.

Figure 7: (a) STEM image and (b) corresponding EDS spectra show a solid nickel seed particle with an amorphous layer of P and O on the exterior surface of the resulting nanoparticle after Ni₂P assisted nanowire growth. EDS 1 represents analysis on the center of the nanoparticle while EDS 2 was taken over the outermost edge of the particle. The Si peak is presumed to be an artifact of TEM analysis.

Figure 8. (a) STEM image and corresponding EDS spectra showing Ti-O nanowire composition grown from Ni₂P seed particle. (b)-(e) EDS line scan across nanowire-nanoparticle interface. Spectra indicate a TiO_x nanowire and solid Ni NP with an amorphous shell of O-rich material at the NW-NP interface.

Figure 9: The Binary phase diagram for Ni-P (adapted from Okamoto15) shows a eutectic temperature of 891°C for a Ni-P mixture that is much lower than the Ni melting temperature at 1455°C.

Figure 1.

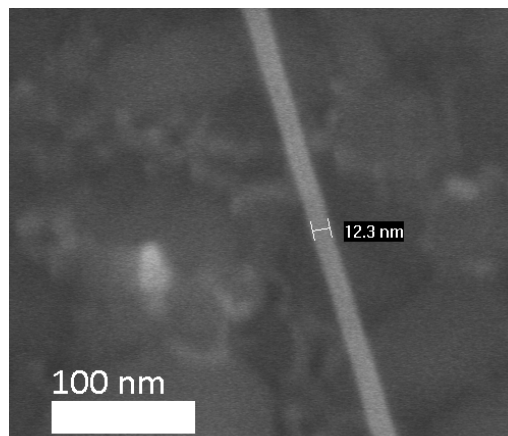


Figure 2.

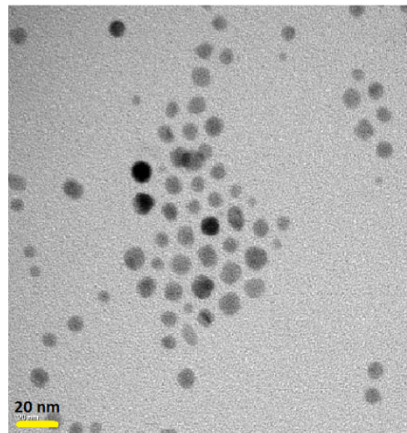


Figure 3.

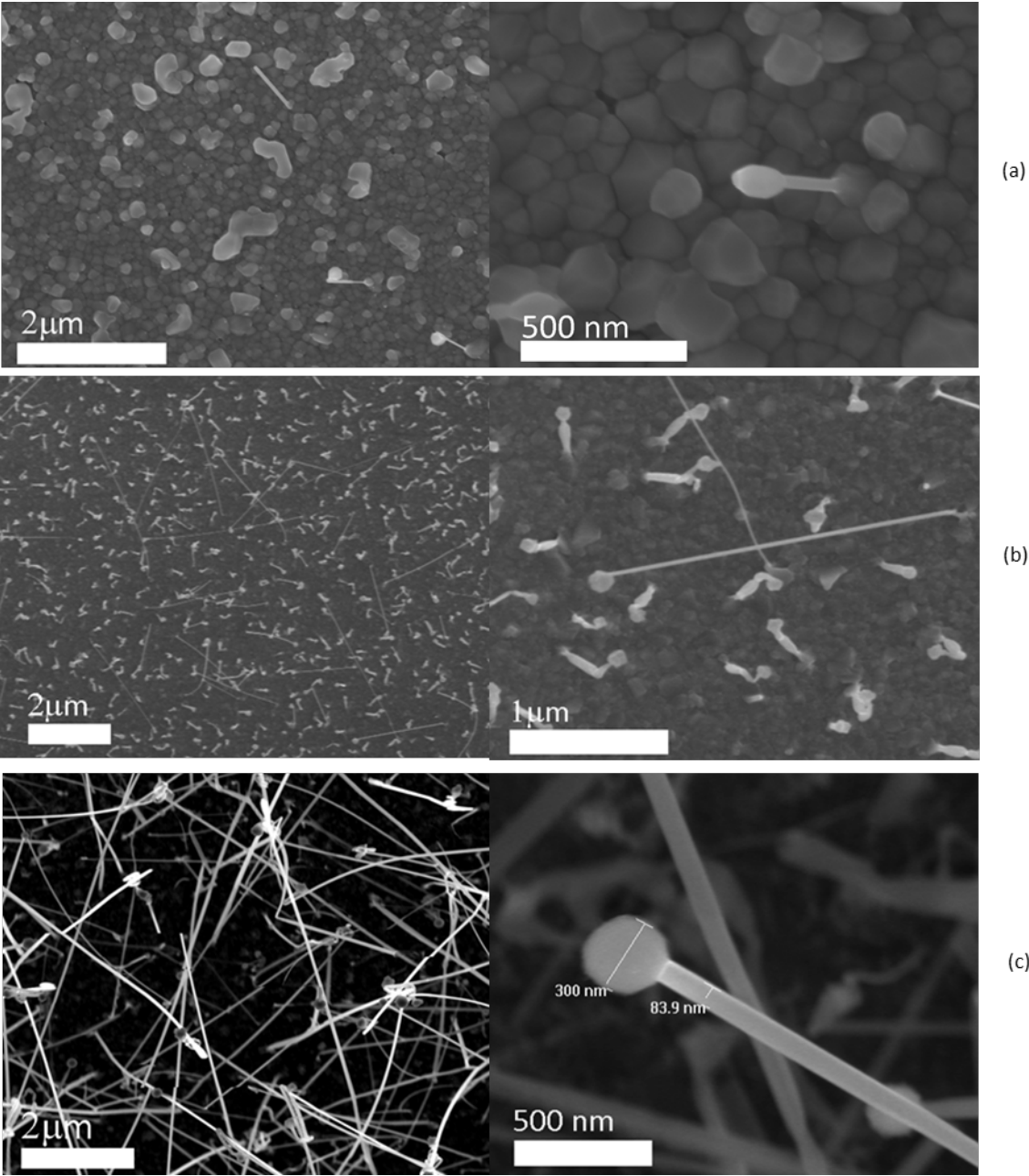


Figure 4.

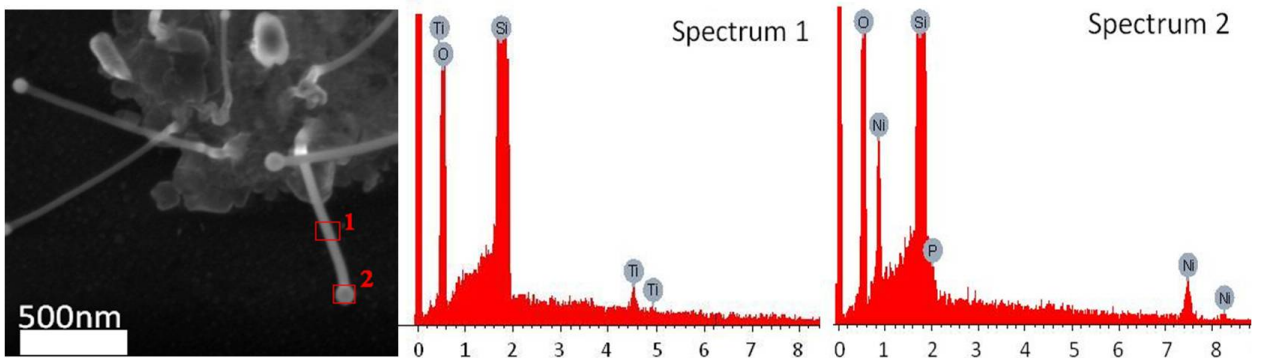


Figure 5.

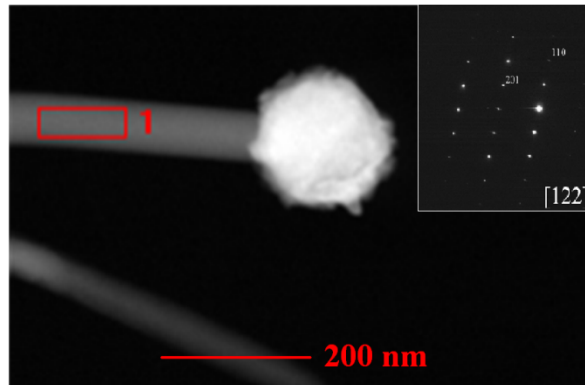


Figure 6.

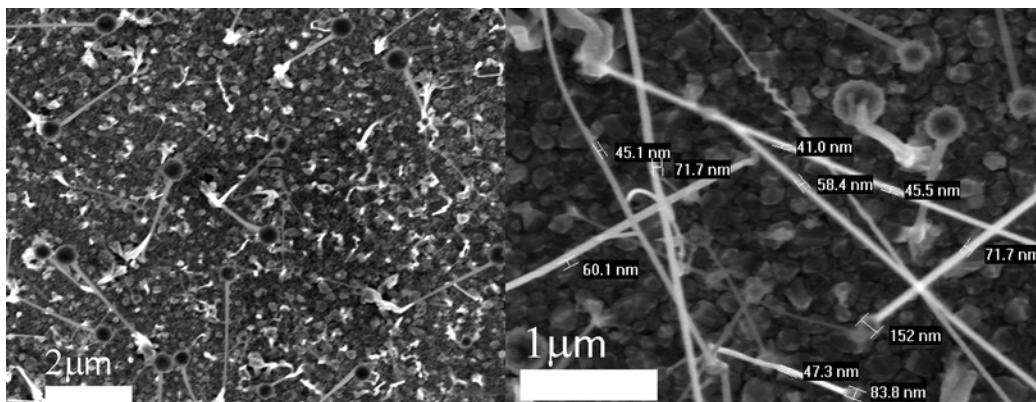


Figure 7.

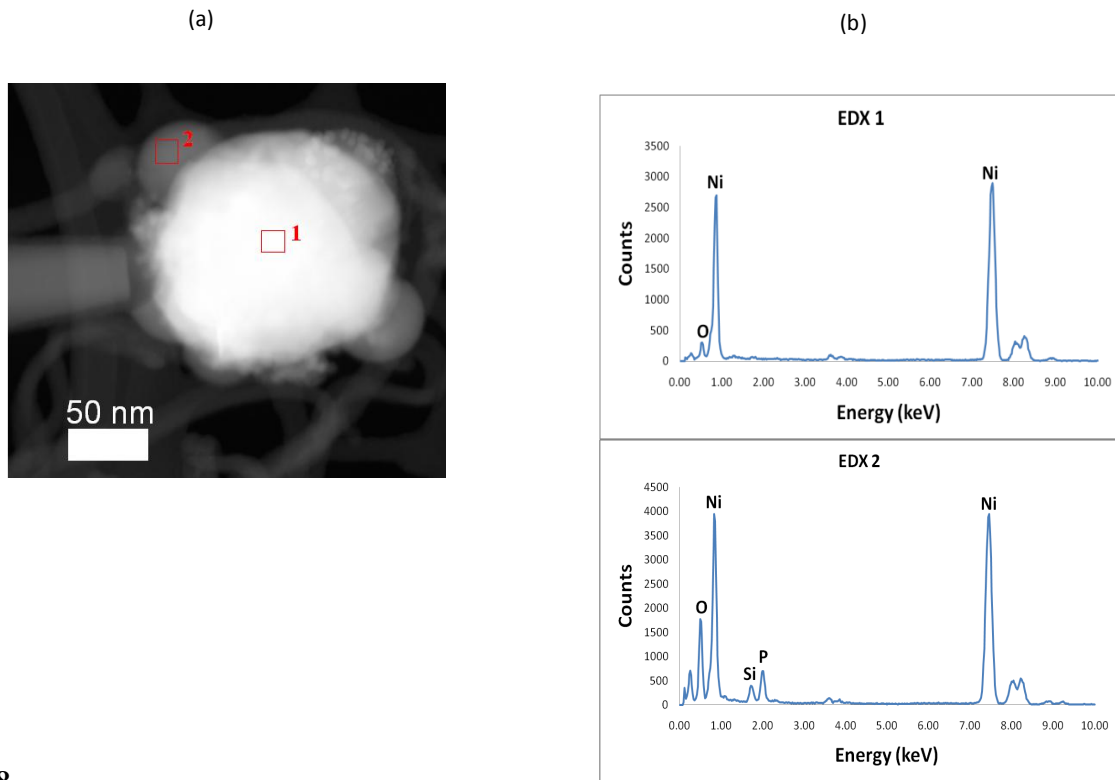


Figure 8.

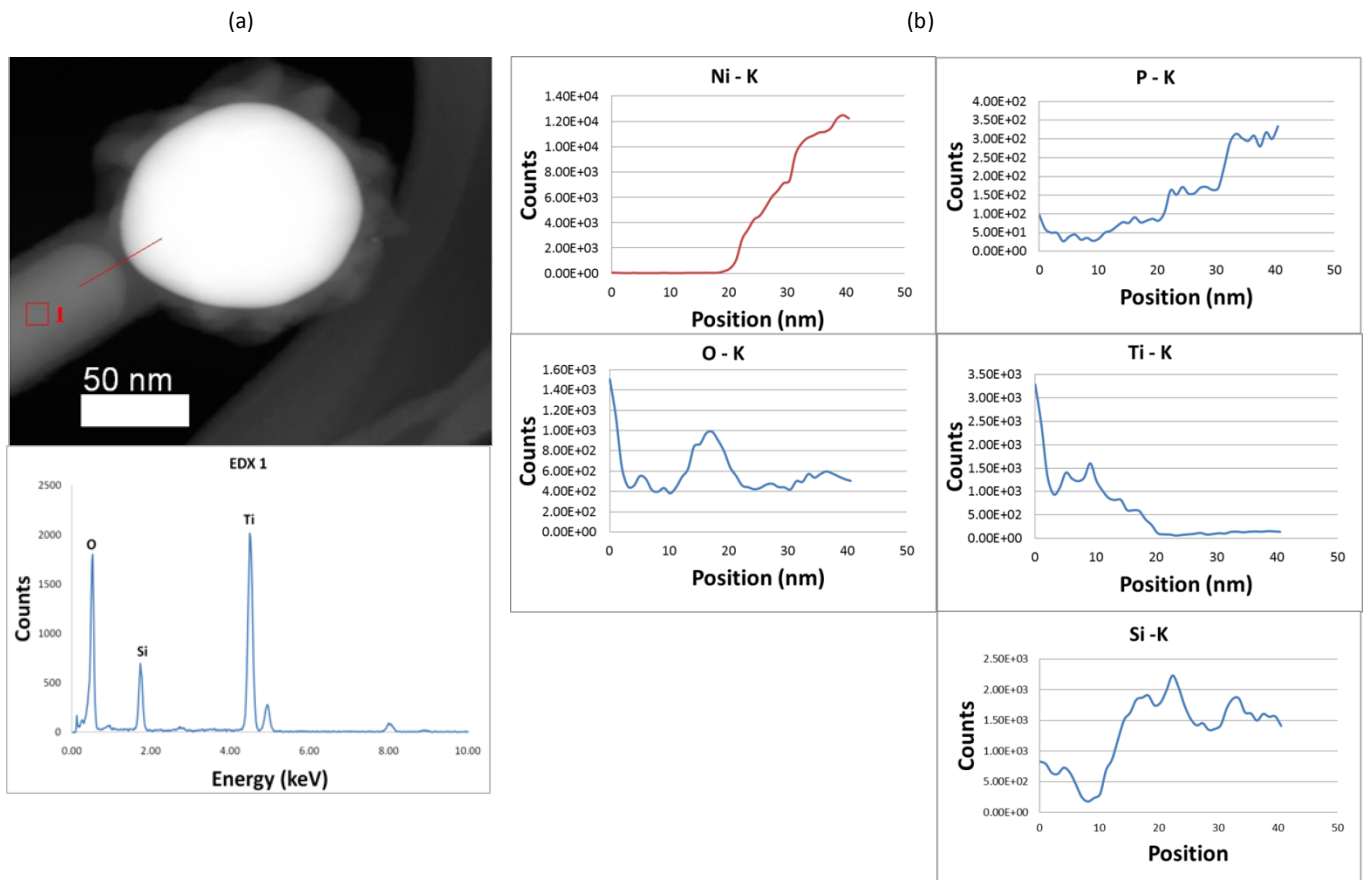


Figure 9.

